Ground Penetrating Radar and Electrical Resistivity Methods to Characterize Soil-Bentonite Slurry Cutoff Wall and Detect Defects

Hannah Elizabeth Rickertsen, Dr. Robert Jacob, Bucknell University, Dept. of Geology & Environmental Geosciences

NS33B
0797
AGU 100 FALL MEETING
Washington, D.C. | 10–14 Dec 2018

Abstract

Soil-bentonite slurry cutoff walls are used to prevent the movement of contaminated groundwater. Defects which reduce the overall efficacy of the wall may become present during construction or the aging of the wall. In this research, we use ground penetrating radar (GPR) and electrical resistivity (ER) as non-invasive and minimally invasive geophysical techniques, respectively, in an attempt to characterize the shallow portions of a soil-bentonite slurry cutoff wall and detect defects within the wall. Sandbags and a limestone block were placed within the northernmost section of an experimental soil-bentonite slurry cutoff wall in Montandon, PA to mimic high hydraulic conductivity defects that may show up in slurry walls during construction or as a wall ages. GPR surveys were collected along the wall and surrounding area to investigate the unsaturated zone and determine if GPR could reliably observe the elevation difference of the water table across the wall. The GPR signal velocity in the unsaturated zone of the cutoff wall is directly related to the soil water content (SWC), and the water table should produce an observable reflection within the GPR profiles. Additionally, GPR signal velocity estimations of SWC differences were also evaluated as a possibly reliable way to determine the location of more permeable zones (e.g., fractures) within the unsaturated zone of the cutoff wall. The apparent resistivity and mutual resistance of both defect and non-defect locations in the wall were collected using long point-source electrodes in Wenner and dipole-dipole arrays at various depths, as well as non-traditional geometries. Additionally, the mise-a-la-masse method with in-wall electrodes and surface electrodes were used to measure the change in voltage along the wall and the surrounding areas in both defect and non-defect locations. We will discuss how data from the individual or concurrent use of these two methods may help locate potential defects within soil-bentonite slurry cutoff walls.

Site Description

Thanks to an NSF grant, an experimental soil-bentonite slurry cutoff wall was installed in Montandon, PA (Figure 1) in the summer of 2016. The wall is 200 m long, about 1 m wide, and 7 m deep (with an additional 30 cm of topsoil added after construction). The first 140 m are reserved for civil engineering stress/strain monitoring during the dewatering process, and the last 60 m reserved for geophysical experimentation[1,2] (Figure 2) . Different size defects made of various materials (limestone and sandbags) were inserted during construction, as shown in Figure 3. This research focused on testing three distinct areas: the area near the limestone block, near the sandbags, and a nondefect location. Each location is color coded in Figure 3, and will henceforth be referred to by the name of the defect in that location. There has been no expected change in the limestone block since it was installed. However, the sandbags were infiltrated with the soil-bentonite slurry as the wall was poured, creating a smaller change in resistivity than what was initially designed for or expected. This makes these sandbag defects harder to detect, as their expected resistivity will be very similar to the surrounding slurry wall.

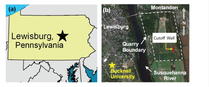

Figure 1. The location of the soil-bentonite slurry cutoff wall, showing its location and proximity to Bucknell University. Image courtesy of M. Malusis.

Figure 2. An overview of the wall, showing the geographic orientation of the wall and the coordinate system used to mark locations. Image courtesy of M. Malusis.

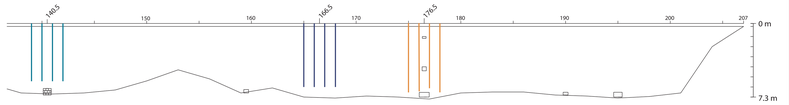

Figure 3. A west-facing cross-section of the soil-bentonite slurry cutoff wall showing the defect initial placement and trench key. The nondefect location is demarcated by a dark blue, the limestone by a teal, and the sandstone by orange. The length of the lines represents how far each electrode was pushed into the ground before refusal.

Background & Methods

Electrical Resistivity

Long point source electrodes were designed and manufactured at Bucknell University based on Pidlesecky, 2006[3]. The metal electrode was attached to PVC pipe which was reinforced with aluminum pipe, then pushed into the ground in 10 cm increments. Each electrode was connected to the Sting R1 Earth Resistivity Meter (AGI) which collected the data (Figure 4 & 5). Each array was centered around the defect (limestone defect array centered at 140.5 m, sandbags defect centered around 176.5 m, see Figure 3). The apparent resistivity (ohm-m) of the wall was directly measured using a Wenner array with an a-spacing of 1 m. Our Wenner apparent resistivity measurements were multiplied by 2, in order to account for the electrodes being fully submerged in the subsurface. The modified equation is shown below in Equation 1:

$$\rho_a = \frac{4\pi\Delta V}{I}\left(\frac{1}{\frac{1}{r_1}-\frac{1}{r_2}-\frac{1}{r_3}+\frac{1}{r_4}}\right)$$

ρ_a is the apparent resistivity (ohm-m)
4π is the geometric factor
$\Delta V/I$ is the mutual resistance
r_n is the distance between different current and potential electrodes within the array

Figure 4. The STING R1 system manufactured by AGI.

This same geometric factor was used by Rucker et al. in their exploration of an industrial site with long electrodes in the subsurface[4].

At the same depth, a dipole-dipole array was used to measure the mutual resistance (ohm). The mutual resistance was then converted to apparent resistivity using Equation 2:

$$\rho_a = \pi n(n+1)(n+2)a\frac{V}{I}$$

ρ_a is the apparent resistivity (ohm-m)
a is the distance between each electrode in the dipole
n is a scaling factor
V/I is the mutual resistance.

Similarly, these results were multiplied by 2 to account for the electrodes being entirely in the subsurface.

Figure 5 (below). Long point source electrodes in the ground at about 3.5 m depth. The electrodes are connected to 1" PVC pipe partially reinforced with aluminum pipe to prevent deflection while being pushed into the ground.

Figure 6. The pulseEKKO Pro system and 500 MHz antennas on sled.

Ground Penetrating Radar

In this research, ground penetrating radar (GPR) was used for reconnaissance only. GPR profiles were taken along the centerline of the slurry wall and perpendicular to it using pulseEKKO Pro (Sensors & Software Inc) 500 MHz and 200 MHz antennas with an antenna spacing of 25 cm and 1 m respectively. These profiles were then processed using a DeWOW filter, SEC2 gain, and other adjustments based on the specific profile. Further and more specific information is in each figure caption.

Electrical Resistivity Data, Analysis & Conclusions

Figures 7 and 8 illustrate what we expected the graphs of apparent resistivity (ohm-m) versus depth (m) to look like for the sandbag defect and limestone defect. These graphs were modeled using a weighted average of the apparent resistivity of the individual materials based on their volume in a representative 1 m^3 volume. The apparent resistivity of the slurry wall was found to be 12.27 ohm-m when the wall was built, and the resistivity of the sandbags at 15% saturation (designed) was found to be 287 ohm-m^5 (designed model). One complication was the infiltration of the slurry mixture into the sandbags, which based on laboratory observations, lowered the resistivity to 43.1 ohm-m^6 (infiltrated model). The resistivity of the limestone was estimated to be about 500 ohm-m, based on porosity and saturation[7,8].

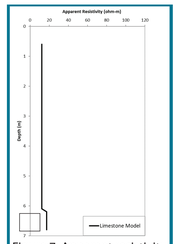

Figure 7. Apparent resistivity versus depth model for limestone defect.

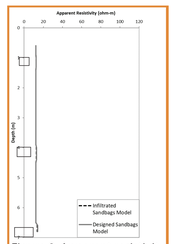

Figure 8. Apparent resistivity versus depth model for sandbag defect.

Wenner Array

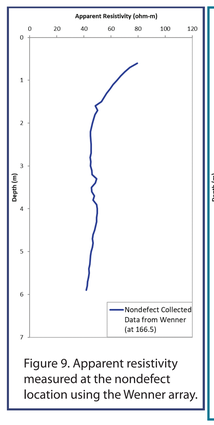

Figure 9. Apparent resistivity measured at the nondefect location using the Wenner array.

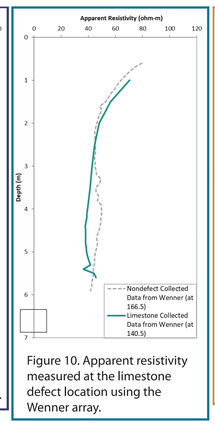

Figure 10. Apparent resistivity measured at the limestone defect location using the Wenner array.

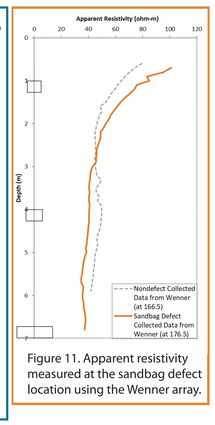

Figure 11. Apparent resistivity measured at the sandbag defect location using the Wenner array.

The initial decrease seen in Figures 9, 10, and 11 is likely due to the increase in water content as the water table is approached. With an increase in water content, the apparent resistivity of the wall will decrease. After 4 m depth, the graphs diverge. We believe these differences in these curves show that there is a change in the material of the wall or the surrounding geology.

Dipole-Dipole Array

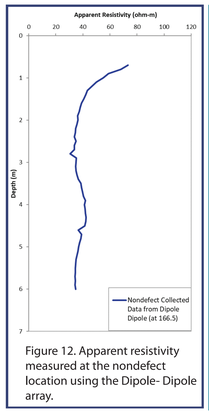

Figure 12. Apparent resistivity measured at the nondefect location using the Dipole- Dipole array.

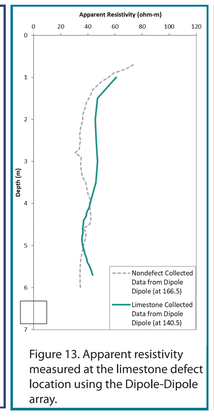

Figure 13. Apparent resistivity measured at the limestone defect location using the Dipole-Dipole array.

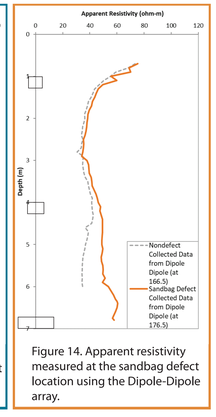

Figure 14. Apparent resistivity measured at the sandbag defect location using the Dipole-Dipole array.

The Dipole-Dipole array data show the same initial steep decrease in resistivity due to a rapid increase in soil water content due to the proximity to the water table. Again, around 4 m depth, the nondefect and defect graphs begin to diverge. Figure 14 shows how the sandbag defect location apparent resistivity increases steadily towards the end of the survey depth, which was expected. Figure 13 shows a decrease in apparent resistivity, which is then followed by an increase (the opposite of the nondefect location data). This anomaly could be due to a regional geology change between the two locations. Figures 15, 16, and 17 all compare the apparent resistivity from the Wenner array (dashed line) and the apparent resistivity as calculated from the mutual resistance collected via the Dipole-Dipole array (solid line). Figure 15 shows the two nondefect plot curves, which match each other well in terms of overall pattern. The offset between the two can be attributed to the difference in the flow of electricity due to the electrode configuration in the array. The Dipole-Dipole array is better at detecting lateral changes in geology, while the Wenner array is better at detecting near-horizontal contacts with increasing depth. Based on Figure 15, we confirmed that the Dipole-Dipole array detected more of the materials within the wall based on the fact that it is closer to the tested value of the soil-bentonite (12.27 ohm-m).

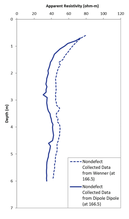

Figure 15.

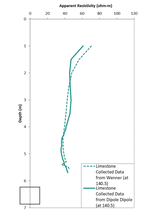

Figure 16.

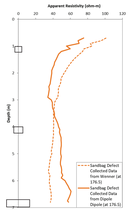

Figure 17.

GPR Data, Analysis & Conclusions

Centerline profiles of the slurry wall were taken with both 200 MHz and 500 MHz antennas. Both profiles show a minimal depth of penetration due to the high attenuation of the GPR signal. Clay is very conductive to EM waves which causes this attenuation. Saturated clay causes the signal to attenuate even more, resulting in a poor depth of penetration. When data was collected, there had been recent rainfall, resulting in the soil water content being high. These material of the wall and the amount of water in the wall both contribute to the poor depth of penetration. The depth on either plot is not sufficient to see to the trench key, and therefore not deep enough to see any of the defects as distinct reflectors. Additionally, Figure 18 shows a 200 MHz profile taken perpendicular to the centerline of the slurry wall. This profile shows little difference between the water content and the composition of the surrounding geology and the slurry wall. As expected, there is no strong reflector at the lateral boundary of the slurry wall.

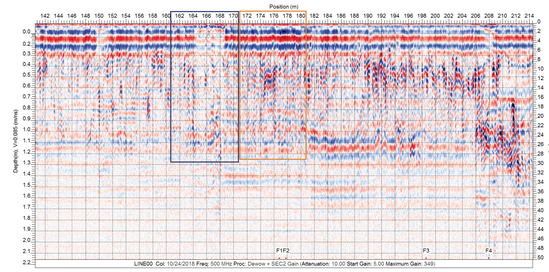

Figure 18. 500 MHz profile of the centerline of the wall. Depth calculated by using a representative subsurface velocity (0.085 m/ns) determined by using diffraction hyperbolas.

Figures 18a and 18b. 500 MHz profile of the slurry wall at the nondefect (blue) and sandbag defect (orange). Defects cannot be seen in this data, however, there may be evidence of the electrode boreholes.

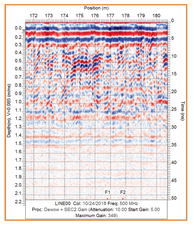

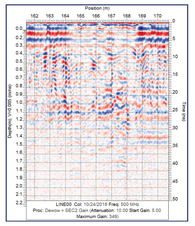

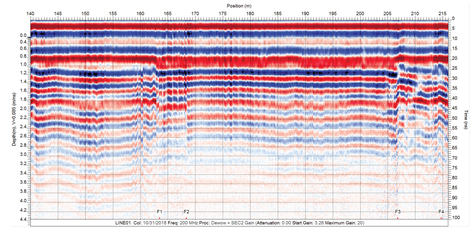

Figure 19 (above). 200 MHz profile of the centerline of the wall. Depth calculated by using the same velocity that was determined in the 500 MHz profile line. This profile does not show any evidence of defects and illustrates the "ringing" affect common in highly conductive materials.

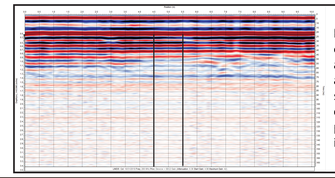

Figure 20. Profile perpendicular to the centerline of the wall using the 200 MHz antennas. The black bold lines show the approximate location of the sides of the slurry walls. Between these lines, there is a decrease in noise in the GPR signal, potentially indicating more homogeneity in the wall than surrounding geology.

Conclusions

- There seems to be a discernible difference in the apparent resistivity versus depth plots of the defect locations from the nondefect locations. This could be due to the defects or a change in the local geology. This could also be reflective of the survey method type.
- The dipole-dipole method seems to be more sensitive to changes potentially located within the wall, as opposed to the Wenner array. These differences are summarized in Figures 13, 14, & 15.
- GPR in this situation with a high clay concentration in the native geology and a high water content, leads to too much attenuation of the GPR signal to yield usable results. The depth of penetration is insufficient to see the defects themselves, however, GPR could still be potentially used to analyze the soil water content on either side of the slurry wall.

Sources & Acknowledgments

Thank you to Dr. Rob Jacob, and the Bucknell University Department of Geology & Environmental Geosciences for making this research possible and for their continuous guidance and support. I am grateful for all of the opportunities this research has provided, as well as all the help I've received along the way (especially in collecting data). A special thank you to the NSF, who provided funding for the construction of the slurry wall.

[1]Malusis, M. A., Evans, J. C., Jacob, R. W., Ruffing, D., Barlow, L., & Marchiori, A. M. (2017). Construction and Monitoring of an Instrumented Soil-Bentonite Cutoff Wall: Field Research Case Study.
[2]Evans, J. C., Ruffing, D. (2017). Design and Construction of an Experimental Soil-Bentonite Cutoff Wall.
[3]Pidlisecky, A., Knight, R., & Haber, E. (2006). Cone-based electrical resistivity tomography. Geophysics, 71(4), G157-G167.
[4]Dale F. Rucker, Meng H. Loke, Marc T. Levitt, and Gillian E. Noonan (2010). "Electrical-resistivity characterization of an industrial site using long electrodes." GEOPHYSICS, 75(4), WA95-WA104. https://doi.org/10.1190/1.3464806
[5]Aborn, Lindsey. (2017). Undergraduate Research Thesis. Bucknell University, Geology & Environmental Geosciences Department.
[6]Warden, Gray. (2018). Independent Research Report. Bucknell University, Geology & Environmental Geosciences Department.
[7]Burger, H. R., Sheehan, A. F., & Jones, C. H. (2006). Introduction to Applied Geophysics: Exploring the Shallow Subsurface. New York: W.W. Norton. pg 325
[8]Telford, W. M., Geldart, L., & Sheriff, R. (1990). Applied Geophysics. Chapter 5: Electrical Properties of Rocks and Minerals